PFC/JA-86-63

Rf Current Generation By Lower Hybrid Slow Waves in the Presence of Fusion Generated Alpha-Particles in the Reactor Regime

Paul Bonoli and Miklos Porkolab

Plasma Fusion Center
Massachusetts Institute of Technology
Cambridge, MA 02139

December 1986

Submitted to: Nuclear Fusion

This work was supported by the U. S. Department of Energy Contract No. DE-AC02-78ET51013. Reproduction, translation, publication, use and disposal, in whole or in part by or for the United States government is permitted.

RF Current Generation By Lower Hybrid Slow Waves in the Presence of Fusion Generated Alpha-Particles in the Reactor Regime

Paul Bonoli and Miklos Porkolab

Plasma Fusion Center
Massachusetts Institute of Technology
Cambridge, MA 02139
USA

Abstract

It is shown that efficient RF current generation using lower hybrid slow waves is possible in the presence of fusion generated alpha-particles. Wave accessibility and the condition for strong quasi-linear electron Landau damping restrict propagation of the slow wave to $r/a \gtrsim 0.5$ in a thermonuclear plasma. This turns out to be a beneficial effect in terms of avoiding significant absorption of the injected waves via alpha-particle damping, because of the spatial peaking of the alpha-particle density profile near the plasma center. Numerical results for RF current generation and wave absorption, relevant to the reactor regime, are obtained using a combined Fokker-Planck and toroidal ray tracing calculation.

I. Introduction

Recent studies [1] of lower hybrid (LH) wave absorption in reactor grade plasmas ($T_e \gtrsim 15$keV and $\overline{n}_e \gtrsim 1 \times 10^{20}\mathrm{m}^{-3}$) have shown that damping of the fast and slow waves will be dominated by absorption on fusion generated alpha-particles. [Here T_e is the electron temperature and $\overline{n}_e$ is the line-average electron density.] This effect would be deleterious to current drive schemes which utilize the lower hybrid wave. In this Letter, it is shown that significant alpha-particle damping of the slow wave can be avoided due to the combined effects of wave accessibility, electron Landau damping, and the peaked nature of the alpha-particle density profile. The restrictions imposed on the parallel refractive index ($n_\parallel$) of the injected LH waves by wave accessibility ($n_\parallel \geq n_a$)[2] and the condition for strong electron Landau damping ($n_\parallel \lesssim n_{\mathrm{eld}}$) limit wave penetration to $r/a \gtrsim 0.5$, for typical reactor parameters. One beneficial aspect of electron Landau damping at $r/a \gtrsim 0.5$

is the mitigation of the effect of alpha-particle damping due to the drop-off of $n_\alpha(r)$ with radius. The LH slow wave would then be useful in applications such as current profile control, including sawtooth stabilization by broadening of the current density profile and hence raising $q(r) > 1$ everywhere, as demonstrated on Asdex [3]. Alternatively, the slow wave still shows promise in lower temperature reactor applications such as plasma start-up and/or combining with electron cyclotron resonance (ECR) current drive or fast wave current drive. A parallel scenario to that proposed in this Letter has been discussed by Andrews and Bhadra [4] for the LH fast wave. In their work it was shown that owing to the combined effects of scattering by density fluctuations near the plasma edge and magnetic shear, the parallel wavenumbers of the injected fast waves would be increased enough so the waves could be absorbed via electron Landau damping at $r/a \gtrsim 0.5$, rather than by alpha-particle damping.

The calculated values of the current drive "figure of merit" $\tilde{\eta} \equiv \overline{n}_e(10^{20}\mathrm{m}^{-3}) \times I_{\mathrm{rf}}(\mathrm{MA}) \times R_o(\mathrm{m})/P_{\mathrm{in}}(\mathrm{MW})$ are found to be quite high [$\tilde{\eta} \lesssim 0.4$ (A/W/m^2)] relative to the existing experiments [5,6] where $\tilde{\eta} \lesssim 0.12$(A/W/m^2). The higher values of $\tilde{\eta}$ are due to two effects. First, the electron temperature is still quite high at $r/a \gtrsim 0.5$ where $\mathrm{T}_e \lesssim 10 - 15$keV for central T_e values of 20–30 keV. Thus LH slow waves with relatively high parallel phase velocities (which are still accessible at $r/a \gtrsim 0.5$) are strongly absorbed due to electron Landau damping [$n_\parallel = n_{\mathrm{eld}} \lesssim 1.8 - 2.2$] on their first pass into the plasma center, resulting in a narrow quasi-linear plateau on the electron distribution function. In present-day experiments, a large 'gap' exists [5,6] in parallel velocity space between the injected LH waves ($n_\parallel \lesssim 1.5, v_\parallel/v_e \gtrsim 10$, and $\mathrm{T}_e \sim 1.5$ keV) and the phase velocities necessary for strong electron Landau damping ($v_\parallel/v_e \sim 2 - 3$ and $n_{\mathrm{eld}} \simeq 5 - 6$). Thus a broad plateau is formed on the electron distribution in these experiments. A consequence of maintaining this quasi-linear plateau at low parallel phase velocity, via Landau interaction with relatively collisional electrons, is a reduction in the driven RF current. A second effect contributing to the higher values of $\tilde{\eta}$ is the pure uni-directionality of the injected Brambilla spectrum [7] that was assumed in these studies. We note that for present day waveguide grill launchers phased at $\pi/2$, approximately 20–30% of the injected power is coupled in the anticurrent drive direction. Hence, it is of interest to develop improved wave launchers for current drive in reactor grade tokamaks.

The plan of this Letter is as follows. Section II is a review of the predictions of wave accessibility and quasi-linear electron Landau damping theory for the reactor scenario

under consideration. A brief review of the radial dependence of the alpha-particle density profile and the alpha-particle absorption theory is also given. Section III outlines the combined Fokker-Planck and toroidal ray tracing model used to calculate the RF current generation. Finally, numerical results are presented in Section IV and the conclusions are given in Section V.

II. Slab Analysis and Review:

The penetration and absorption of LH slow waves can be estimated by recalling that the parallel refractive index of the injected waves must satisfy $n_{\rm eld} \gtrsim n_{\|} \gtrsim n_a$. Here $n_{\rm eld} \approx 7/{\rm T}_e^{\frac{1}{2}}({\rm keV})$ is the maximum value of $n_{\|}$ possible, before wave power is absorbed via strong quasi-linear electron Landau damping (i.e., $v_{\|} = c/n_{\|} \lesssim (2-3) \times v_e$, where $v_e^2 = 2{\rm T}_e/{\rm m}_e$) [8] and n_a is the minimum value of $n_{\|}$ the wave must have in order to propagate to a specified electron density, i.e., [2]

$$n_a = \epsilon_{\perp}^{1/2} + \omega_{pe}/\omega_{ce}, \tag{1}$$
$$\epsilon_{\perp} = 1 + (\omega_{pe}/\omega_{ce})^2 - (\omega_{pi}/\omega_0)^2.$$

Here $\omega_{pe} = (4\pi n_e e^2/{\rm m}_e)^{\frac{1}{2}}$ is the electron plasma frequency, $\omega_{pi}^2 = \sum_{j={\rm D,T}} (4\pi n_j e_j^2 Z_j^2/m_j)$, is the square of the ion plasma frequency and the summation is over the deuterium (D) and tritium (T) ion species, $\omega_{ce} = eB_o/m_e c$ is the electron gyrofrequency, and the range or 'window' of $n_{\|}$ values that satisfies $n_{\rm eld} \gtrsim n_{\|} \gtrsim n_a$ becomes quite narrow for the slow wave in a thermonuclear plasma. This point is illustrated in Fig. 1 where $n_{\rm eld}$ and n_a have been plotted versus r/a assuming profiles of the form

$$T_e(r) = (T_{eo} - T_{ea})(1 - r^2/a^2)^{\gamma_t} + T_{ea}, \tag{2a}$$

$$n_e(r) = (n_{eo} - n_{ea})(1 - r^2/a^2)^{\gamma_n} + n_{ea}. \tag{2b}$$

Figure 1 was obtained for parameters typical of the TIBER-II ETR scenario [9] with $B_\phi = 6{\rm T}$, $f_o = 4.6{\rm GHz}$, ${\rm T}_{eo} = 30{\rm keV}$, ${\rm T}_{ea} = 0.5{\rm keV}$, $n_{eo} = 1.7 \times 10^{20}{\rm m}^{-3}$, $n_{ea} = 0.1 \times n_{eo}$, $n_{eo} = 1.5 \times \overline{n}_e$, $\gamma_n = 1.21$, $\gamma_t = 1.0$, 50% deuterium and 50% tritium mixture. Wave propagtion without severe electron Landau damping is only possible for $r/a \gtrsim 0.6$.

The strength of the alpha-particle damping of LH slow waves as a function of plasma minor radius can be estimated by first considering the alpha-particle density function.

Following the treatment of Ref. [1], the alpha-particle production rate can be balanced against the slowing down of alphas due to electron drag to obtain,

$$n_\alpha(r) = \tau_s^{(\alpha/e)} n_D n_T \langle\sigma v\rangle_{DT}, \tag{3a}$$

where the reaction rate is given by [10]

$$\langle\sigma v\rangle_{DT} = \frac{3.68\times10^{-12}}{\mathrm{T}_D^{2/3}} \exp\left(-\frac{20}{\mathrm{T}_D^{1/3}}\right) \mathrm{cm}^3/\mathrm{sec}. \tag{3b}$$

Here T_D is the deuterium temperature expressed in units of keV. The radial peaking of $n_\alpha(r)$ is a consequence of the exponential factor in $\langle\sigma v\rangle_{DT}$. It is important to remember this form for $n_\alpha(r)$ was derived assuming the slowing down of alpha-particles is dominated by electron drag and the $\tau_s^{(\alpha/e)}$ is therefore independent of alpha-particle energy (E_α), i.e.,

$$\tau_s^{(\alpha/e)} = 1.98\times10^{13} A_\alpha T_e^{3/2}/(n_e Z_e^2 \lambda_{ie}) \tag{4}$$

Here, $A_\alpha = m_\alpha/m_p, \lambda_{ie}$ is the Coulomb logarithm, $T_e = T_e(\mathrm{keV})$, and $n_e = n_e(\mathrm{cm}^{-3})$. Equation (4) is appropriate provided $E_\alpha \gtrsim E_c$, where [11]

$$E_c = 14.68 A_\alpha T_e([\mathrm{Z}])^{2/3}, \tag{5}$$

$$[Z] = (n_D Z_D^2/A_D + n_T Z_T^2/A_T)/n_e,$$

defines the critical energy at which the electrons and ions contribute equally to the slowing down of the alpha-particles. For $Z_D = Z_T = 1, n_D = n_T = 0.5\times n_e, A_D = 2,$ and $A_T = 3$, we have $E_c \simeq 33\times T_e$. It must be required that $E_{\mathrm{rf}} = \frac{1}{2} m_\alpha v_{\mathrm{rf}}^2 \gtrsim E_c$, where E_{rf} is the energy of an alpha particle which a LH slow wave at velocity $v_{\mathrm{rf}} = c/(n_\perp^2 + n_\parallel^2)^{1/2}$ can interact with. For the parameters in Fig. 1 this condition is marginally satisfied at r=0 and well-satisfied at $r/a \gtrsim 0.25$.

The wave damping due to the alpha-particles is obtained by starting with the form for $f_\alpha(\mathbf{v})$, valid for $E_\alpha \gtrsim E_c$ [11],

$$f_\alpha(\mathbf{v}) = \frac{f_o}{v^3 + v_c^3}, \tag{6}$$

where $E_c = \frac{1}{2} m_\alpha v_c^2$ and the alphas are assumed to be borne isotropically at an energy $E_0 = 3.5$ MeV and remain isotropic as they slow down. The normalization f_o is determined by using Eqs. (3a) and (6) in the definition of particle density, i.e.,

$$n_\alpha(r) = \int_0^{2\pi} d\phi \int_{-1}^{+1} d\mu \int_{v_c}^{v_0} v^2 f_\alpha(v) dv,$$

where $\mu = v_\parallel/v$ is the pitch-angle, $v^2 = v_\perp^2 + v_\parallel^2$, and $E_0 = \frac{1}{2}m_\alpha v_0^2$. This yields,

$$f_0 \simeq \frac{\langle\sigma v\rangle_{DT} n_D n_T \tau_s^{(\alpha/e)}}{2\pi \ln[0.63(v_0/v_c)^2]}. \tag{7}$$

Assuming unmagnetized alpha-particles [$(k_\perp \rho_\alpha)^2 \gg 1$, where $\rho_\alpha = v_\alpha/\Omega_{c\alpha}$], the damping can then be calculated from the imaginary part of the susceptibility,

$$\chi_\alpha = \frac{1}{n_\alpha}\frac{\omega_{p\alpha}^2}{k^2}\int_L \frac{du\partial F_{\alpha 0}/\partial u}{\omega/k - u}, \tag{8a}$$

$$F_{\alpha 0}(u) = \int d\mathbf{v} f_\alpha(\mathbf{v})\delta(u - \mathbf{k}\cdot\mathbf{v}/k), \tag{8b}$$

where the integral in Eq. (8a) is evaluated along the Landau contour. Using Eq.(6) in (8b) yields $F_{\alpha 0} = 2\pi f_0/u$. Using this result in Eq.(8a) one obtains

$$\mathrm{Im}(\chi_\alpha) = -\pi\frac{\omega_{p\alpha}^2}{\omega^2}/\ln[0.63(v_0/v_c)^2]. \tag{9}$$

III. Current Drive Simulation Model

The simulation model used in the following calculations has been described in detail in Ref. [12]. In brief, the current drive model incorporates a toroidal ray tracing code and a one-dimensional (parallel velocity) Fokker-Planck calculation. The toroidal ray tracing utilizes a Shafranov equilibrium for the magnetic field with shifted, circular flux surfaces. The wave damping along each ray trajectory is calculated for quasi-linear electron Landau damping, linear ion Landau damping, (assuming unmagnetized ions), nonresonant damping (due to electron-ion Coulomb collisions), and Landau damping on fusion generated alpha-particles (see Sec. II). The self-consistent RF diffusion coefficient is calculated based on the local rate of quasi-linear electron Landau damping. The Fokker-Planck calculation is relativistically correct for parallel velocity, includes the effect of an arbitrary perpendicular electron temperature $T_\perp$, due to pitch-angle scattering, and also contains an electron tail loss model. The Fokker-Planck equation is solved assuming steady state ($\partial F_e/\partial t = 0$), where $F_e(r, v_\parallel)$ is the electron distribution function, and the DC electric field ($E_\parallel$) is neglected since it is sufficiently small relative to the runaway electric field.

IV. Numerical Results

A. The results of a central electron temperature scan are shown in Table I for parameters characteristic of the TIBER–II ETR scenario. $T_e(r)$ and $n_e(r)$ are given by Eqs. (2a) and (2b) with $T_{eo} = (2-30)$keV, $T_{ea} = 0.5$keV (except for $T_{eo} = 2keV$ where $T_{ea} = 0.05$keV), $T_i(r) = T_e(r)$, $n_{eo} = 1.7 \times 10^{20}\mathrm{m}^{-3}, n_{ea} = 0.1 \times n_{eo}, n_{eo} = 1.5 \times \overline{n}_e, \gamma_n = 1.21$ and $\gamma_t = 1.0$. Other parameters are $a = 1.24m, R_0 = 3m, I_p = 10$MA, $q_0 = 1.0, B_\phi = 6$T, 50%/50% D–T gas mixture, $\omega_0/2\pi = 4.6$GHz, $T_\perp = T_e$, and electron tail confinement time is set by $\tau_L = (1 \text{ sec.})\gamma^3$. The injected RF power spectrum is calculated according to

$$\begin{aligned} s(n_\parallel) &= s_0 \exp[-\alpha_p(n_\parallel - \overline{n}_\parallel)^2], \qquad n_\parallel > 0 \\ &= 0, \qquad\qquad\qquad\qquad\quad n_\parallel < 0 \end{aligned}$$

where $\alpha_p = 32$, $\overline{n}_\parallel = 1.5$, and s_0 is chosen so that $\int_{-\infty}^{\infty} s(n_\parallel) dn_\parallel = P_{in} = 45$MW. The initial power spectrum is divided into 50 rays with spacing $\Delta n_\parallel = 0.044$ for $1.066 \leq n_\parallel \leq 1.99$ and $\Delta n_\parallel = 0.22$ for $1.99 \leq n_\parallel \leq 8.37$. The rays are launched from a poloidal location of $\theta_0 = 3\pi/2$, corresponding to the bottom of the tokamak.

From Table I, it can be seen that the figure of merit remains high [$\tilde{\eta} \gtrsim 0.3(A/W/m^2)$] for $T_{eo} \gtrsim 15$keV but then drops by a factor of three for $T_{eo} = 2$keV. The power absorbed due to alpha-particle damping is $P_\alpha \lesssim 2.8$ MW and the power absorbed due to quasi-linear electron Landau damping is $P_e \lesssim 42$MW. The power lost via nonresonant collisional damping at the plasma periphery is small for $T_{eo} \gtrsim 15$keV with $P_{\mathrm{coll}} \lesssim 0.1$ MW but becomes significant for $T_{eo} \simeq 2$keV where $P_{\mathrm{coll}} = 9.6$ MW. The power lost because of imperfect electron tail confinement is low, with $P_L \lesssim 0.03$ MW, and the remaining RF power $(P_e - P_L)$ is dissipated in the bulk plasma via the collisional slowing down of fast tail electrons. The higher collisional damping in the $T_{eo} = 2$keV case occurs because the LH ray trajectories are not damping on their first pass into the plasma. The rays require additional radial reflections at the plasma edge in order to induce toroidal upshifts in $n_\parallel$ [12] ($n_\parallel = 4-6$ is required for electron Landau damping in this case). The maxima in the radial profiles of electron Landau damping and alpha-particle damping are given in Table I by $r^{(e)}_{\mathrm{max}}$ and $r^{(i)}_{\mathrm{max}}$ respectively. Although $r^{(e)}_{\mathrm{max}} \simeq 67\mathrm{cm} \gtrsim 0.5 \times a$ for the $T_{eo} = 2$keV case, LH waves are still able to propagate to $r/a \lesssim 0.25$ since $n_a = 1.85$ and $n_{\mathrm{eld}} = 4.95$ at the plasma center. The wave absorption via electron Landau damping is peaked at 67 cm because of the broadness of the $T_e(r)$ profile, i.e., $T_e(r^{(e)}_{\mathrm{max}}) \simeq 1.45$keV for $T_{eo} = 2$keV.

The radial profiles of electron Landau damping and RF current generation for the 30 keV case are shown in Figs. 2(a) and 2 (b). The electron distribution function for $v_\parallel > 0$

and at a radial location $r_{\max}^{(e)} = 97$cm is plotted in Fig 2 (c) as a function of parallel kinetic energy $E = m_e c^2[n_\parallel/(n_\parallel^2 - 1)^{1/2} - 1]$. The plateau extends from $E \simeq 60$keV corresponding to $n_\parallel = n_{\rm eld} \simeq 2.24$, to $E \simeq 200$keV corresponding to $n_\parallel \approx 1.44$, in good agreement with the restrictions imposed by wave accessibility. This is to be contrasted with the $T_{eo} = 2$keV case where the electron tail extends from 13 keV to 200 keV at $r = r_{\max}^{(e)}$.

The RF current profile shown in Fig. 2(b) is not expected to change because of the radial diffusion or transport of suprathermal current carrying electrons.[13] This is easily seen to be the case because the slowing down time of an electron at energy 160 keV and electron density $n_e \simeq 8 \times 10^{19}\mathrm{m}^{-3}$ is $\tau_s \lesssim 4 \times 10^{-3}$ sec. However, a typical diffusion time scale in a reactor might be $\tau_d \lesssim \tau_e \lesssim 1$ sec. Thus $\tau_d \gg \tau_s$ and suprathermal electrons are thermalized before they can diffuse spatially.

A typical ray trajectory for the $T_{eo} = 30$keV is shown in Fig. 3(a) for an initial value of $n_\parallel = n_\parallel^0 = 1.4$. The normalized minor radial position (ρ/a) is plotted versus toroidal angle (ϕ) in Fig. 3(b). Here $\rho = r + \Delta(r)\cos\theta$ and $\Delta(r)$ is the Shafranov shift. The parallel refractive index $(n_\parallel)$ and normalized power amplitude of the ray (P_n) have also been plotted versus toroidal angle in Figs. 3(c) and 3(d). The value of $n_\parallel$ increases initially along the ray path with a final value of $n_\parallel \simeq 1.8$. Approximately 8% of the RF power along this ray was absorbed due to alpha-particle damping and the remaining 92% of the power was absorbed via quasi-linear electron Landau damping.

B. The effects of significant alpha-particle damping can be demonstrated by using the parameters of the previous part, setting $T_{eo} = T_{io} = 15$keV and raising the magnetic field to $B_\phi = 12T$, so that accessibility is achieved for even low values of $n_\parallel$. The range of $n_\parallel$ values accessible to the plasma center is now $1.34 \leq n_\parallel \leq 1.81$ where $n_a = 1.34$ and $n_{\rm eld} = 1.81$. Table II contains the results of such a study with $\overline{n}_\parallel = 1.2, 1.3$, and 1.5. As $\overline{n}_\parallel$ is reduced form 1.5 to 1.2, the LH waves propagate nearer to the plasma center because the lower initial $n_\parallel$ values help to keep $n_\parallel < n_{\rm eld}$. However, the absorption of the LH waves on alpha-particles increases significantly, until at $\overline{n}_\parallel = 1.2$ almost half of the injected RF power is absorbed at $0 \lesssim r \lesssim 50$ cm via this damping mechanism. Consequently, the electron Landau damping and RF current generation for the $\overline{n}_\parallel = 1.2$ case occur only at $30\mathrm{cm} \lesssim r \lesssim 80\mathrm{cm}$ with maxima at $r_{\max}^{(e)} \simeq 57$cm.

V. Conclusions

It has been shown that LH slow waves can be used to generate RF current in a thermonuclear plasma ($\overline{n}_e \gtrsim 1 \times 10^{20}\mathrm{m}^{-3}$ and $T_{eo} \gtrsim 15\mathrm{keV}$) at $r/a \gtrsim 0.5$, thus avoiding significant absorption of the injected waves on fusion generated alpha-particles. The figure of merit for the proposed scenario [$\tilde{\eta} \lesssim 0.4(A/W/m^2)$] is considerably higher than in present-day experiments [$\tilde{\eta} \lesssim 0.12(A/W/m^2)$]. The LH slow wave should therefore be considered as potentially useful in a reactor-grade plasma for RF current maintenance at $r/a \gtrsim 0.5$ and to achieve sawtooth stabilization via current profile control.

Acknowledgements

We acknowledge useful discussions with Dr. B. Grant Logan, Dr. R. S. DeVoto, and Dr. M. Fenstermacher. This work was supported by the U. S. Department of Energy under contract No. DE-AC02-78ET51013.

Table I

Electron Temperature Scan: TIBER-II Lower Hybrid Current Drive Parameters.

T_{eo} (keV)	I_{rf} (MA)	$\tilde{\eta}$ (A/W/m^2)	P_α (MW)	$r^{(e)}_{max}$(cm)	$r^{(i)}_{max}$(cm)
2	1.24	0.09	0.03	67	10
15	4.06	0.31	2.1	91	70
20	4.86	0.37	2.2	91	74→90
30	4.98	0.38	2.8	97	97

Table II

Scan for Alpha-particle damping effects: Tiber-II

Lower Hybrid Current Drive Parameters.

$\overline{n}_\parallel$	I_{rf} (MA)	$\tilde{\eta}$ (A/W/m^2)	P_α (MW)	$r^{(e)}_{max}$(cm)	$r^{(i)}_{max}$(cm)
1.2	2.05	0.15	22.6	57	0→50
1.3	3.4	0.26	10.1	76	60
1.5	2.67	0.20	2.0	70	79

REFERENCES

[1] Wong, K. L., Ono, M., Nucl. Fusion **24** (1984) 615.

[2] Porkolab, M., in **Fusion**, ed. by E. Teller, Academic Press, New York (1981) Vol 1B 151.

[3] Söldner, F., et al., Phys. Rev. Lett. **57** (1986) 1137.

[4] Andrews, P. L., Bhadra, D. K., Nucl. Fusion **26** (1986) 897.

[5] Bernabei, S., Daughney, C., Efthimion, P., Hooke, W., Hosea, J., Jobes, R., Martin, A., Mazzucato, E., Meservey, E., Motley, R., Stevens, J., Von Goeler, S., Wilson, R., Phys. Rev. Lett. **49** (1982) 1255.

[6] Porkolab, M., Schuss, J. J., Lloyd, B., Takase, Y., Texter, S., Bonoli, P. T., Fiore, C., Gandy, R., Gwinn, D., Lipschultz, B., Marmar, E., Pappas, D., Parker, R., Pribyl, P., Phys. Rev. Lett. **53** (1984) 450.

[7] Brambilla, M., Nucl. Fusion **16** (1976) 47.

[8] Brambilla, M., in **Physics of Plasmas Close to Thermonuclear Conditions** (Int. School of Plasma Physics, CEC, 1980) Vol I 291.

[9] Henning, C. D., Logan, B. G., Perkins, L. J., Barr, W. L., Bulmer, R. H., DeVoto, R. S., Doggett, J. N., Fenstermacher, M. E., Johnston, B. M., Lee, J. D., Miller, J. R., Slack, D. S., Summers, L., Bull. Am. Phys. Soc. **31** (1986) 1504.

[10] Glasstone, S., Lovberg, R. H., **Controlled Thermonuclear Reactions**, Van Nostrand, New York (1960) 20.

[11] Anderson, D., Hamnen, H., Lisak, M., Phys. Fluids **25** (1982) 353.

[12] Bonoli, P. T., Englade, R. C., Phys. Fluids **29** (1986) 2937.

[13] Englade, R., Bonoli, P. T., in **Radiofrequency Plasma Heating**, ed. by D. G. Swanson, AIP, New York (1985) 151.

Figure Captions

Fig. 1 n_{eld} and n_a versus r/a for the parameters of Sec. II (T_{eo} = 30keV, $n_{eo} = 1.7 \times 10^{20}\mathrm{m}^{-3}$, $\omega_0/2\pi = 4.6$GHz, and $\mathrm{B}_\phi = 6$T).

Fig. 2 Simulation model results for T_{eo} = 30keV case in Table I of Sec. IIIA. (a) Radial profile of RF power deposition to electrons ($\mathrm{W/cm^3}$). (b) Radial profile of RF current density ($\mathrm{kA/cm^2}$). (c) Electron distribution function at a radial location r = 97 cm versus parallel kinetic energy E.

Fig. 3 Ray trajectory for T_{eo} = 30keV case in Table I of Sec. IIIA. (a) Projection of the ray trajectory in the poloidal plane of the tokamak. (b) Variation in ρ/a versus toroidal angle (ϕ). (c) Variation in parallel refractive index ($n_\parallel$) versus toroidal angle (ϕ). Initially, $n_\parallel = 1.4$. (d) Normalized wave amplitude (P_n) that results from damping on the quasi-linear electron distribution function ($n_\parallel > 0$), versus toroidal angle (ϕ).

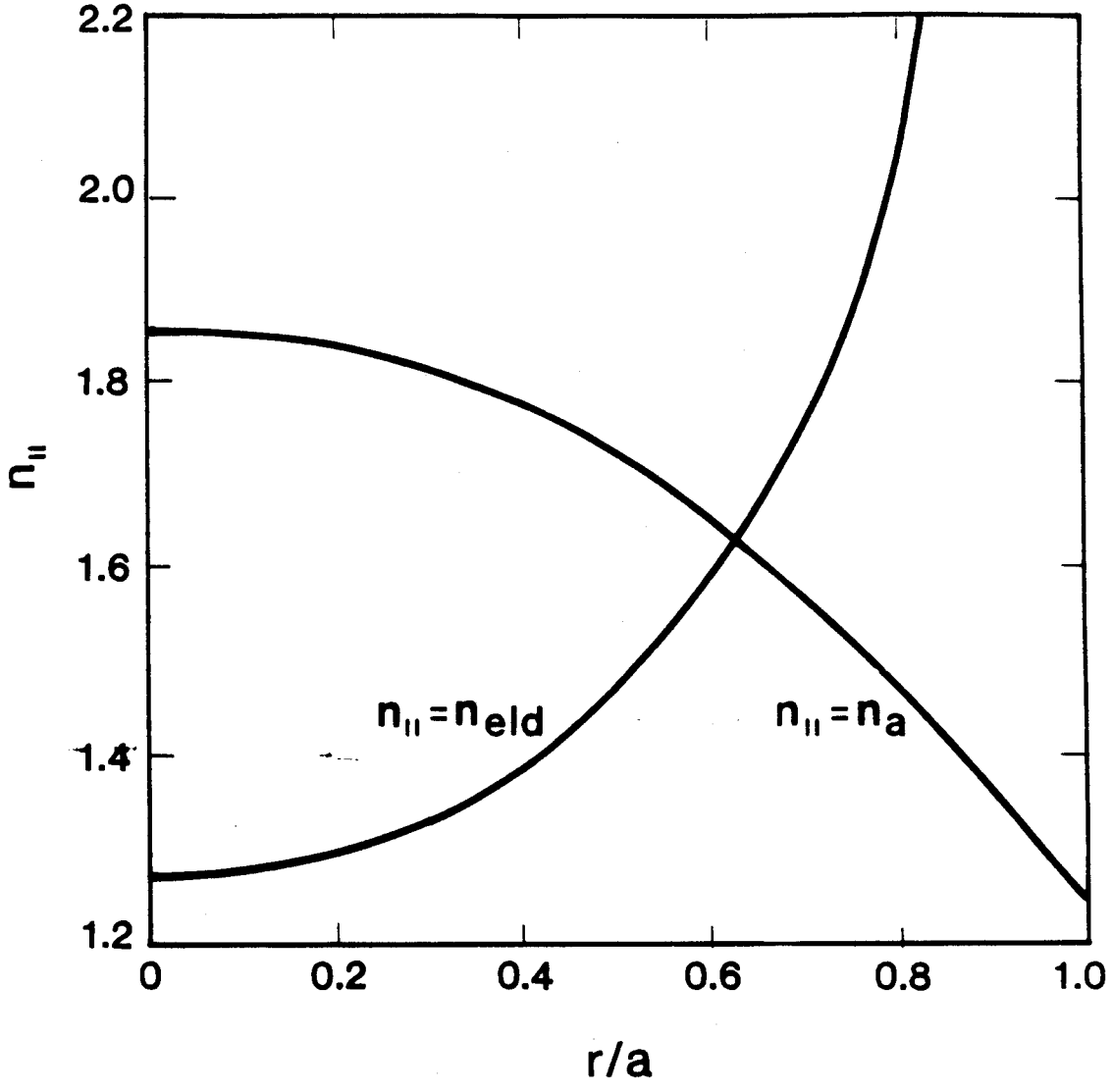

Figure 1

8712-5-2

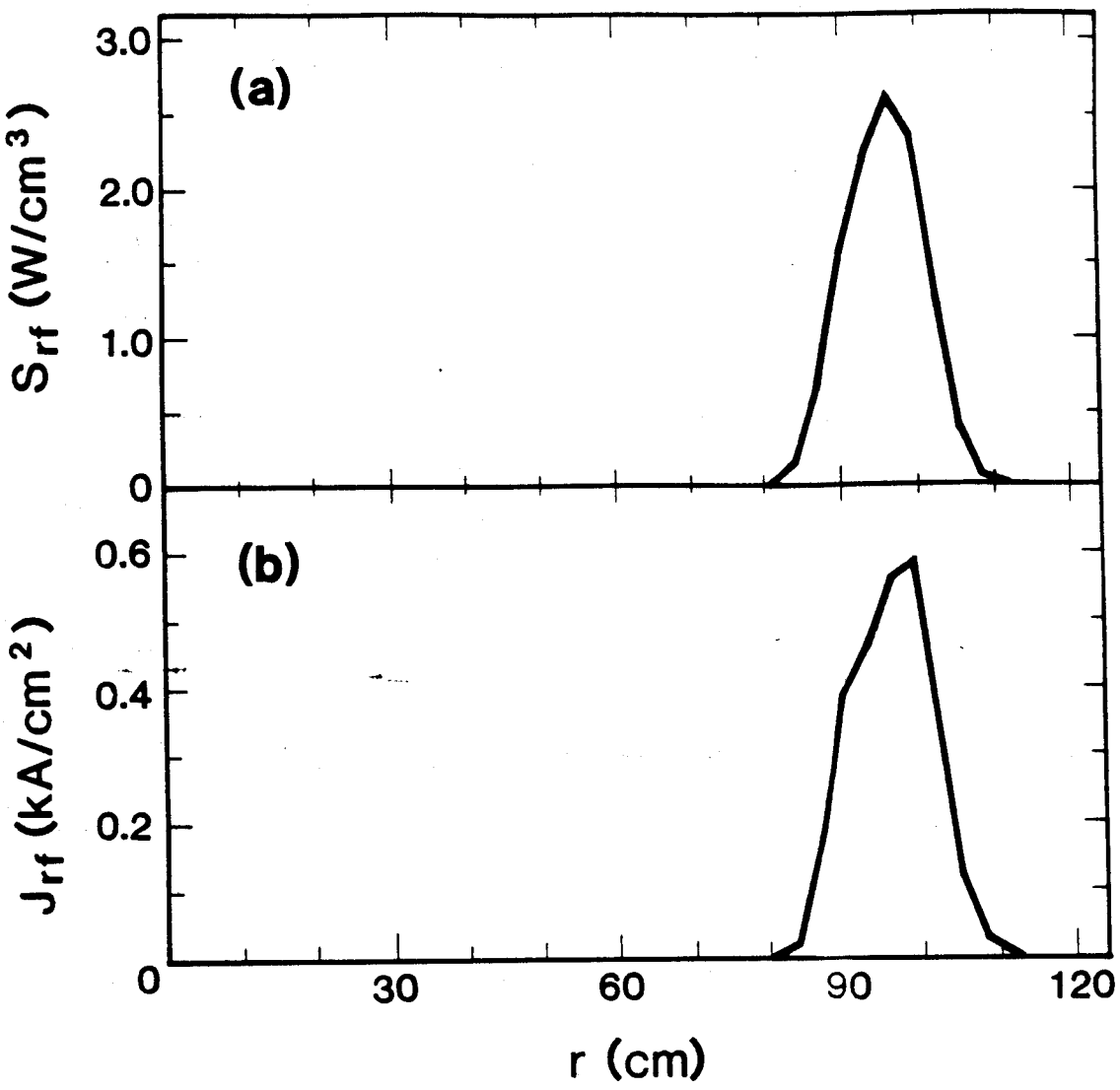

Figure 2(a)-2(b)

87/2.5.5

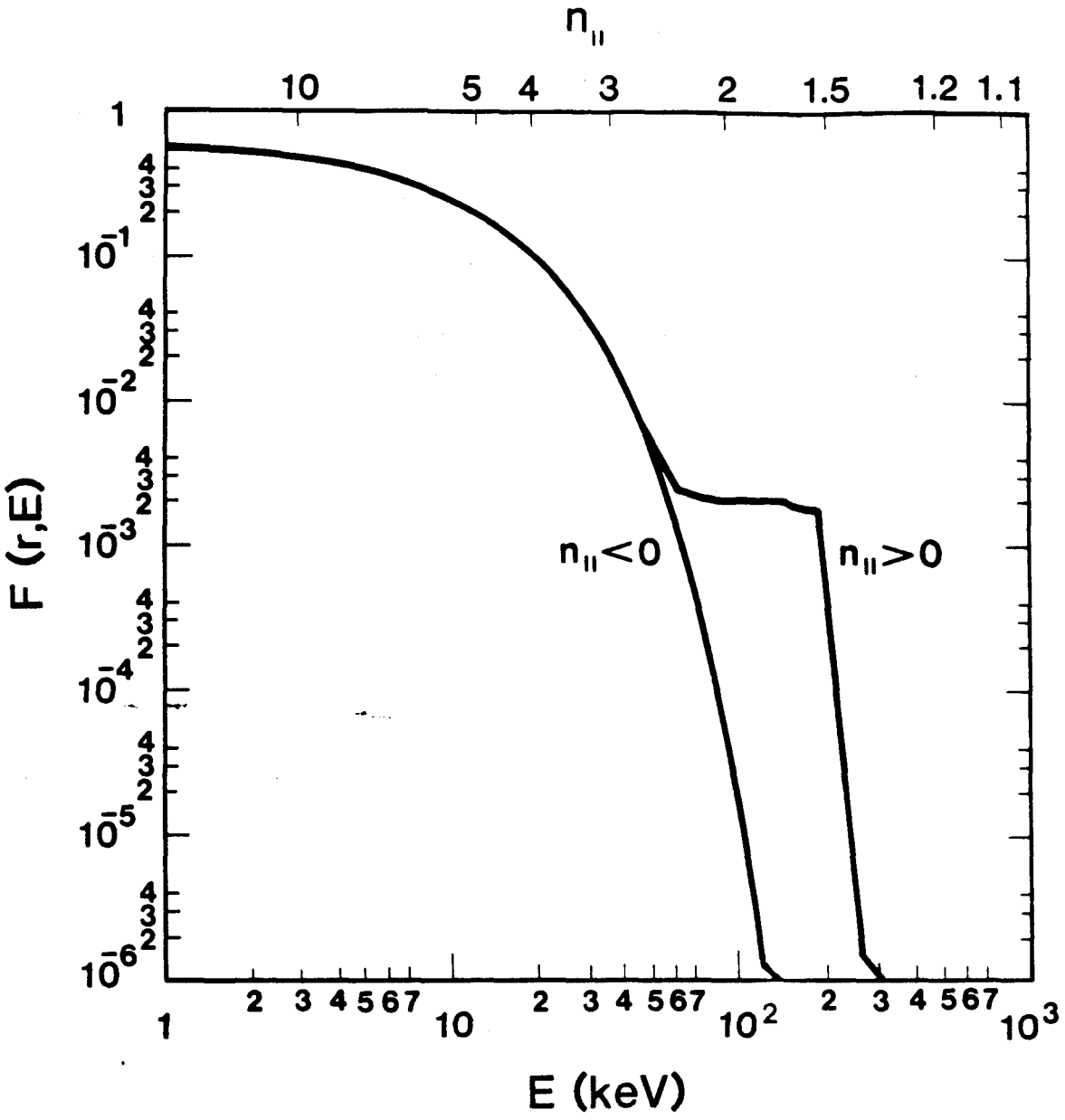

Figure 2(c)

8712 5.4

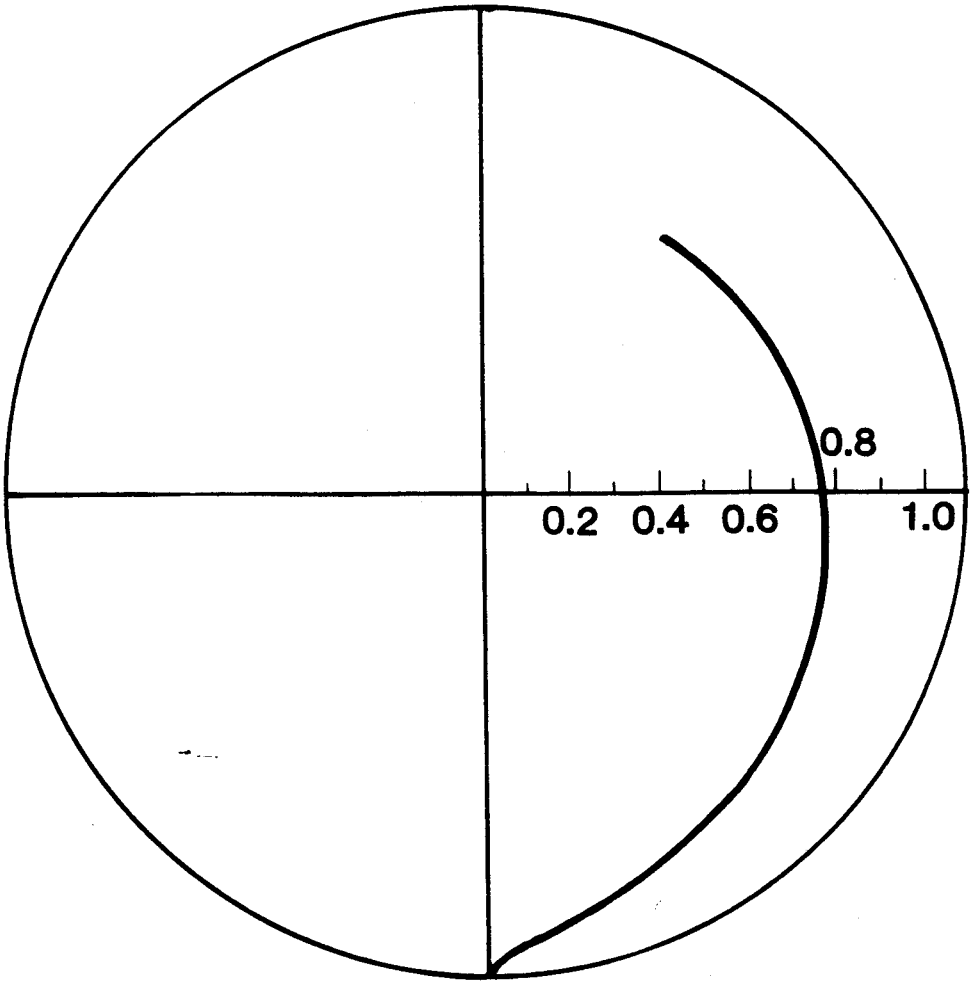

Figure 3(a)

87/2.5.3

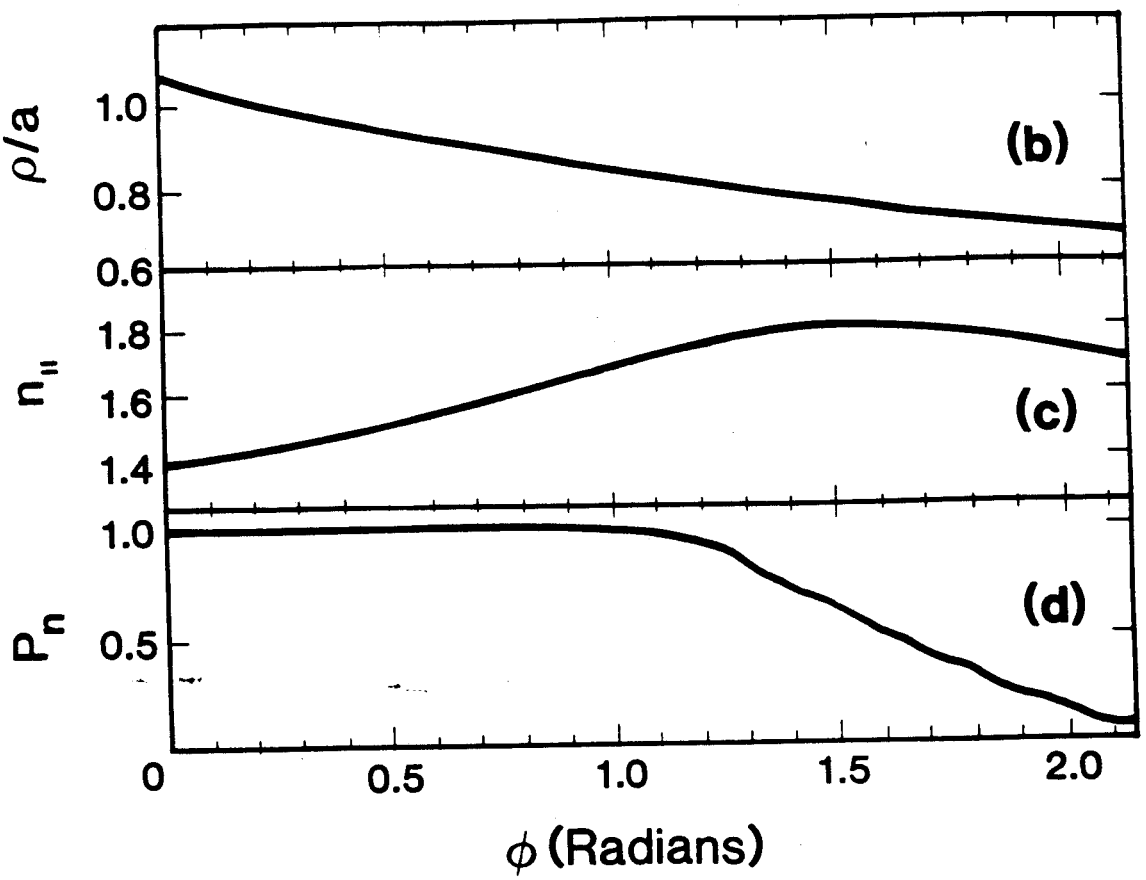

Figure 3(b)-3(d)

8712.5-1